THE JOURNAL OF PHYSICAL CHEMISTRY LETTERS
A JOURNAL OF THE AMERICAN CHEMICAL SOCIETY

pubs.acs.org/JPCL Letter

Jumping Kinetic Monte Carlo: Fast and Accurate Simulations of Partially Delocalized Charge Transport in Organic Semiconductors

Jacob T. Willson, William Liu, Daniel Balzer, and Ivan Kassal*

Cite This: *J. Phys. Chem. Lett.* 2023, 14, 3757−3764 Read Online

ACCESS | Metrics & More | Article Recommendations | Supporting Information

ABSTRACT: Developing devices using disordered organic semiconductors requires accurate and practical models of charge transport. In these materials, charge transport occurs through partially delocalized states in an intermediate regime between localized hopping and delocalized band conduction. Partial delocalization can increase mobilities by orders of magnitude compared to those with conventional hopping, making it important for the design of materials and devices. Although delocalization, disorder, and polaron formation can be described using delocalized kinetic Monte Carlo (dKMC), it is a computationally expensive method. Here, we develop jumping kinetic Monte Carlo (jKMC), a model that approaches the accuracy of dKMC for modest amounts of delocalization (such as those found in disordered organic semiconductors), with a computational cost comparable to that of conventional hopping. jKMC achieves its computational performance by modeling conduction using identical spherical polarons, yielding a simple delocalization correction to the Marcus hopping rate that allows polarons to jump over their nearest neighbors. jKMC can be used in regimes of partial delocalization inaccessible to dKMC to show that modest delocalization can increase mobilities by as much as 2 orders of magnitude.

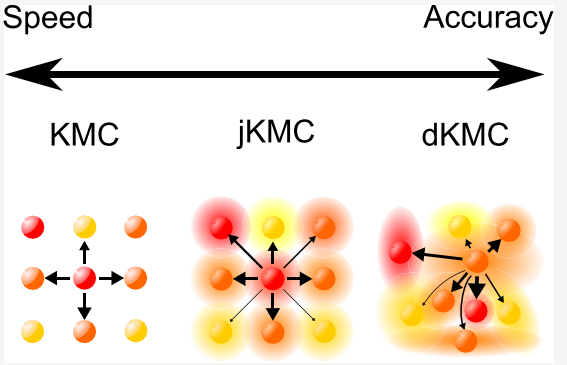

Charge transport is easily modeled in perfectly ordered materials, where charges travel in delocalized bands, and in perfectly disordered ones, where localized charges hop from one site to another. However, many promising materials, such as organic semiconductors, lie in the intermediate transport regime, where charge transport occurs by hops between partially delocalized states.[1−3] In these materials, both static disorder[4] and polaron formation[5] localize charges, and partially delocalized states arise when this localization is insufficient to reduce the state to one molecule. Understanding intermediate-regime transport is especially important in organic semiconductors, where it underpins the most conductive disordered materials and devices.[6,7]

State-of-the-art models of partially delocalized charge transport use quantum-mechanical treatments, which can make them computationally expensive. The most detailed models are atomistic simulations such as fragment orbital-based surface hopping[6,8−10] and coupled electron−ion dynamics.[11,12] Coarse-graining to reduce computational cost gives effective-Hamiltonian models[13] such as transient localization,[14,15] an adaptive hierarchy of pure states equations,[16] density matrix renormalization group approaches,[17,18] network approaches,[19,20] modified Redfield approaches,[21] and polaron-transformed Redfield approaches.[22,23] Nevertheless, the computational cost of these models limits them to small systems (usually in one or two dimensions) or short time scales. Recently, we developed delocalized kinetic Monte Carlo (dKMC), a quantum-mechanical model that can describe charge transport in disordered materials on mesoscopic scales and in three dimensions while including the three essential ingredients: disorder, partial delocalization, and polaron formation.[3,24] dKMC demonstrates the importance of delocalization in disordered charge transport, explaining order-of-magnitude increases in mobility over that of conventional hopping.[3] However, despite the large computational savings of dKMC compared to other quantum-mechanical treatments, it remains expensive, making it impractical for simulations of highly delocalized states in three dimensions or on device scales, where the cost scales exponentially with the number of particles.

Here, we develop jumping kinetic Monte Carlo (jKMC), a practical model of intermediate-regime charge transport of modestly delocalized carriers, whose speed is comparable to that of hopping models and whose accuracy is comparable to that of dKMC. We do so by treating the partially delocalized states as a lattice of identical, spherical polarons (Figure 1), allowing us to avoid the most computationally expensive aspects of dKMC. The result of jKMC is a simple

Received: February 11, 2023
Accepted: April 6, 2023

https://doi.org/10.1021/acs.jpclett.3c00388
J. Phys. Chem. Lett. 2023, 14, 3757−3764

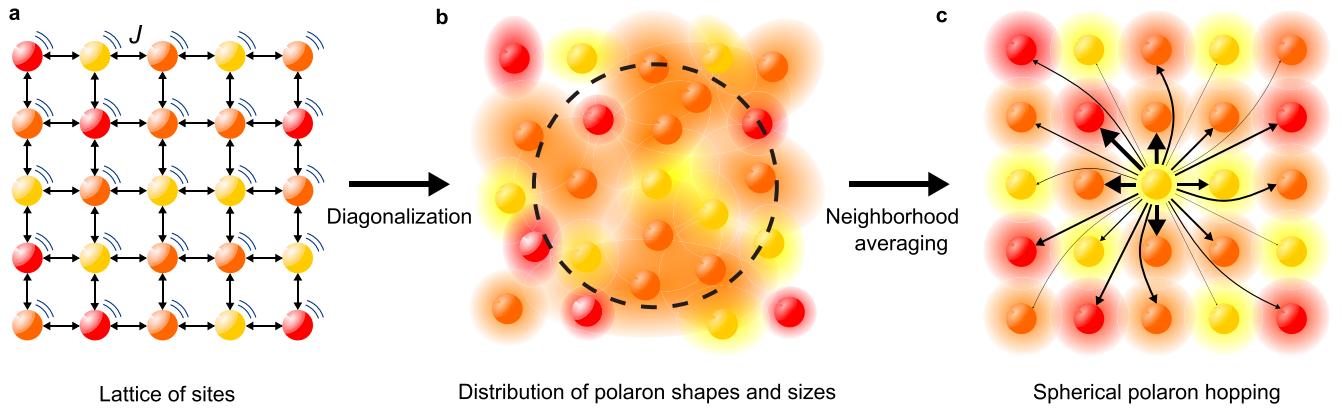

Figure 1. jKMC model of partially delocalized charge transport in disordered materials. (a) The starting point of jKMC is a lattice of sites with disordered energies (different colors) and nearest-neighbor couplings J, coupled to the environment (motion lines). (b) Diagonalizing the Hamiltonian yields delocalized polarons with a distribution of shapes and sizes. A suitably chosen neighborhood (dashed line) is used to average the polaron sizes into a uniform size for jKMC. (c) jKMC uses the neighborhood-averaged polaron size to represent partially delocalized transport as hopping between uniformly sized spherical polarons. This delocalization allows polarons to jump over their nearest neighbors.

delocalization correction to the Marcus hopping rate that can be included in any transport model. Applied to charge transport, it reveals even greater mobility enhancements for states that are too delocalized to be modeled in dKMC.

Conventional models of charge transport in disordered materials commonly use kinetic Monte Carlo (KMC) simulations to model hopping between an array of sites, usually a lattice. Disorder is commonly introduced by assigning to each site an independent random energy from a Gaussian density of states (DOS) of width σ.[1,25] The probability of each hop and the time taken are determined by the hopping rates, usually expressed using nearest-neighbor Marcus or Miller–Abrahams rates

$$k_{if}^{\text{Marcus}} = \frac{2\pi J^2}{\sqrt{4\pi\lambda k_B T}} \exp\left[-\frac{(E_f - E_i + \lambda)^2}{4\lambda k_B T}\right] \tag{1}$$

$$k_{if}^{\text{MA}} = \begin{cases} \nu_0 e^{-(E_f - E_i)/k_B T} & \text{if } E_f > E_i \\ \nu_0 & \text{otherwise} \end{cases} \tag{2}$$

where J is the electronic coupling between neighboring sites, λ is the reorganization energy, ν_0 is the hopping attempt frequency, T is the temperature, E_i and E_f are the energies of the initial and final sites, respectively,[26,27] and we have set $\hbar = 1$. These rates are widely used due to their simplicity, low computational cost, and ability to explain, for example, the electric-field and temperature dependence of mobilities in certain disordered materials.[25,28−31]

The nearest-neighbor rates presented above are often modified to model partially delocalized charge transport by using them to simulate non-nearest-neighbor hopping. To do so, k_{if}^{Marcus} and k_{if}^{MA} are usually multiplied by a phenomenological tunnelling factor, $e^{-2\gamma d_{if}}$, where γ is a fitting parameter called the inverse localization radius and d_{if} is the hopping distance.[25,27,30] The tunnelling factor was originally developed for impurity conduction in crystalline materials, where it correctly captures the overlap of exponentially decaying tails of distant impurity sites. However, this justification is not valid for densely packed organic semiconductors,[32] where there are many sites in the proximity of each other. However, we will see that jKMC results in an expression similar to the tunnelling factor for realistic amounts of delocalization in organic semiconductors.

Instead of a phenomenological factor, dKMC models the fundamental processes giving rise to partially delocalized transport.[3] dKMC uses the secular polaron-transformed Redfield equation (sPTRE) to model transport between delocalized polarons.[23] It assumes an effective, tight-binding Hamiltonian for a lattice of sites, where each site is linearly coupled to an identical, independent bath of harmonic oscillators. The polaron transformation is applied to this Hamiltonian, reducing the system−bath coupling and allowing it to be treated by second-order perturbative Redfield theory. Applying this treatment to a system with normally distributed energies and nearest-neighbor electronic couplings J yields the rate of hopping from polaron ν to polaron ν'

$$R_{\nu\nu'} = \sum_{\langle i,j\rangle,\langle i',j'\rangle} 2J^2 \text{Re}[\langle\nu|i\rangle\langle j|\nu'\rangle\langle\nu'|i'\rangle\langle j'|\nu\rangle K_{\Delta(ij,i'j')}(\omega_{\nu\nu'})] \tag{3}$$

where ν and ν' are eigenstates of the polaron-transformed Hamiltonian, $\langle i, j\rangle$ and $\langle i', j'\rangle$ are nearest-neighbor pairs of sites, $\omega_{\nu\nu'} = E_\nu - E_{\nu'}$ is the energy difference between the polarons, and $K_{\Delta(ij,i'j')}(\omega)$ describes the residual system−bath coupling in the polaron frame, as described in section S1 of the Supporting Information. In calculating $K_{\Delta(ij,i'j')}(\omega)$, we assume a super-ohmic spectral density $J(\omega) = \frac{\pi\lambda}{4}(\omega/\omega_c)^3 e^{-\omega/\omega_c}$, where λ is the reorganization energy and the cutoff frequency (ω_c) is set to 62 meV.[23] This spectral density is commonly assumed for disordered organic semiconductors;[22,33−35] however, any spectral density can be employed.

Calculating the hopping rate $R_{\nu\nu'}$ in dKMC requires diagonalizing disordered Hamiltonians to calculate the delocalized polaron states $|\nu\rangle$, which have irregular shapes and off-lattice positions. Diagonalizing these Hamiltonians becomes the computational bottleneck for dKMC in three dimensions, and at large J values, the states become too large to be contained within a Hamiltonian that can be diagonalized.

jKMC avoids the computational bottleneck of dKMC by avoiding the calculation of all of the polaron states. Instead, it assumes that the polaron wave functions are identical and spherically symmetric. We also assume that the polarons are centered on a cubic lattice with spacing a and have independent and normally distributed energies (with a mean

https://doi.org/10.1021/acs.jpclett.3c00388
J. Phys. Chem. Lett. 2023, 14, 3757−3764

of 0 and a standard deviation of σ) and that their shapes follow the exponential localization seen in the Anderson model.[4] Specifically, we take

$$|\nu\rangle = A \sum_i \exp\left(-\frac{d_{i\nu}}{r_{\text{deloc}}}\right)|i\rangle \tag{4}$$

where $d_{i\nu}$ is the distance between the center of polaron ν and site i, r_{deloc} is the delocalization radius that characterizes the size of the wave function, and $A = [\sum_i \exp(-2d_{i\nu}/r_{\text{deloc}})]^{-1/2}$ is the normalization.

Parametrizing jKMC requires choosing a value of r_{deloc}. Our objective is to choose the r_{deloc} that will yield accurate mobilities. In disordered materials, r_{deloc} should depend on mean energy $\langle E\rangle$ of the polarons because polaron sizes decrease (on average) as they relax to more localized states lower in the disordered DOS. For example, r_{deloc} should be larger for an ensemble of randomly occupied polaron states (where $\langle E\rangle = 0$ and many large states in the middle of the DOS are occupied) than for an ensemble of polarons that have reached thermal equilibrium (where $\langle E\rangle = -\sigma^2/k_BT$ and the occupied states are mostly the localized traps).[1]

To choose r_{deloc}, we relate it to a readily calculated measure of delocalization, the inverse participation ratio

$$\text{IPR}_\nu = \left(\sum_i |\langle i|\nu\rangle|^4\right)^{-1} \tag{5}$$

which roughly equals the number of sites over which polaron ν is delocalized. A localized wave function has an IPR of 1, while a wave function evenly spread across N sites ($\langle i|\nu\rangle = N^{-1/2}$) has an IPR of N. The spherical polarons of eq 4 have an IPR of

$$\text{IPR}_{\text{jKMC}} = A^{-4}\left[\sum_i \exp\left(-\frac{4d_{i\nu}}{r_{\text{deloc}}}\right)\right]^{-1} \tag{6}$$

an equation that allows us to calculate an r_{deloc} that reproduces a given IPR.

We set r_{deloc} using eq 6 on the basis of the mean IPR of the polaron states that participate in charge transport at a given $\langle E\rangle$. This IPR is calculated through an approach we call neighborhood averaging. First, we note that the averaging of the polaron IPRs should be thermally weighted because transport is driven by relaxation to thermal equilibrium. A complete thermal average requires that every state be accessible; however, during the initial stages of transport in a disordered material, the polaron is unable to completely explore the DOS. Instead, if a polaron can explore only a local neighborhood of N polaron states until a particular time, we take the thermal averages of polaron states within that neighborhood. Therefore, we define the effective IPR and the effective energy as

$$\text{IPR}_{\text{eff}}(N) = \left\langle \frac{1}{Z}\sum_{\nu=1}^{N} \text{IPR}_\nu \exp\left(-\frac{E_\nu}{k_BT}\right)\right\rangle \tag{7}$$

$$E_{\text{eff}}(N) = \left\langle \frac{1}{Z}\sum_{\nu=1}^{N} E_\nu \exp\left(-\frac{E_\nu}{k_BT}\right)\right\rangle \tag{8}$$

where IPR_ν and E_ν are the polaron IPRs and energies, respectively, obtained from the diagonalization of the model Hamiltonian,[3] $Z = \sum_{\nu=1}^{N} \exp(-E_\nu/k_BT)$ is the partition function, and the average (angle brackets) is taken over an ensemble of disordered energetic landscapes (1000 instances in our calculations). Equations 7 and 8 allow us to obtain an r_{deloc} for any $\langle E\rangle$ in two steps. First, for a given $\langle E\rangle$, we determine the appropriate neighborhood size N using eq 8, and second, we use that same N in eq 7 to determine the IPR_{eff} that can be converted into r_{deloc} using eq 6.

With r_{deloc} in hand, we can now substitute the spherical-polaron approximation in eq 4 into the delocalized polaron hopping rate (eq 3). To obtain a simple rate expression, we also assume the high-temperature limit ($k_BT \gg \omega_c$), because many organic semiconductors operate close to this limit.[36−38] In addition, the high-temperature limit is the regime of validity of ordinary Marcus theory, and using it reveals the relationship between ordinary KMC and jKMC. Using the spherical-polaron and high-temperature approximations, we obtain the jKMC rate between any two polarons (derivation in section S1 of the Supporting Information)

$$k_{\nu\nu'}^{\text{jKMC}} = k_{\nu\nu'}^{\text{Marcus}}\xi_{\nu\nu'} \tag{9}$$

where $k_{\nu\nu'}^{\text{Marcus}}$ is the Marcus rate of eq 1 from polaron ν to ν' as if they were nearest neighbors and $\xi_{\nu\nu'}$ is the delocalization correction

$$\xi_{\nu\nu'} = A^4 \sum_{\langle i,j\rangle} \exp\left[-\frac{2(d_{i\nu} + d_{j\nu'})}{r_{\text{deloc}}}\right] \tag{10}$$

where the sum runs over nearest-neighbor pairs of sites i and j. Hence, the effect of delocalization is to make Marcus rates long-range in a way that depends straightforwardly on delocalization radius r_{deloc}.

In the low-delocalization limit, $\xi_{\nu\nu'}$ can be simplified by taking only the dominant exponential terms in eq 10, which leads to the simplified jKMC rate (derivation in section S2 of the Supporting Information)

$$\xi_{\nu\nu'}^{\text{simplified}} = \frac{d_{\nu\nu'}}{a}\exp\left[-\frac{2(d_{\nu\nu'} - a)}{r_{\text{deloc}}}\right] \tag{11}$$

Simplified jKMC is similar to inserting the phenomenological correction $e^{-2\gamma d_{if}}$ into the Marcus rate and can be considered as a rigorous justification of this correction in the limit of small delocalization. However, there are two important differences. First, the distance-dependent exponent is offset by the lattice constant, which ensures that the correct Marcus rate is reproduced for nearest neighbors. Second, there is a new pre-exponential factor $d_{\nu\nu'}/a$ that accounts for the number of terms significantly contributing to the sum in eq 10.

The jKMC rates $k_{\nu\nu'}^{\text{jKMC}}$ can now be used to simulate polaron dynamics. Disordered materials show dispersive transport (mobilities decreasing over time as the polarons relax within the DOS),[31,37,39,40] which affects how mobilities should be calculated. Conventionally, mobilities in dispersive systems have been calculated at a chosen time t_μ (Figure 2a); however, this approach can lead to unrealistic comparisons, because it can predict lower mobilities for systems with stronger couplings J, where polarons can reach deeper traps in the DOS within the same t_μ. To avoid this pitfall, we calculate the mobilities of polarons that have relaxed (on average) to a chosen target energy E_μ [i.e., for which $\langle E\rangle = E_\mu$ (see Figure 2b)]. In particular, in jKMC, we choose the value of r_{deloc} that is consistent with this target E_μ.

https://doi.org/10.1021/acs.jpclett.3c00388
J. Phys. Chem. Lett. 2023, 14, 3757−3764

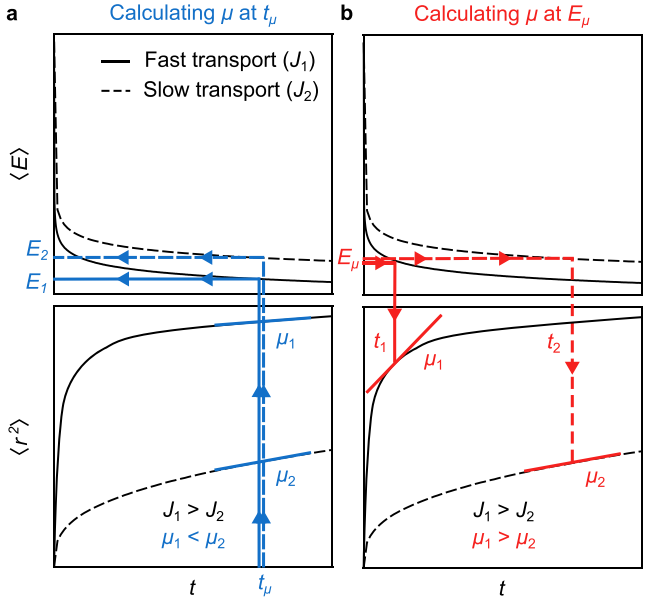

Figure 2. Calculating mobilities at a target energy. (a) Conventionally, mobilities in dispersive materials are calculated at a particular time t_μ from the slope of mean-squared displacement $\langle r^2 \rangle$ as a function of time. This approach can unrealistically predict smaller mobilities for carriers with higher electronic couplings J because polarons with larger J values can move faster and reach deeper traps in the DOS ($E_1 < E_2$) within a given t_μ. (b) This problem is avoided by calculating mobilities at a particular energy E_μ. Here, the mobilities are calculated at times t_1 and t_2 when the respective simulations reach the target energy.

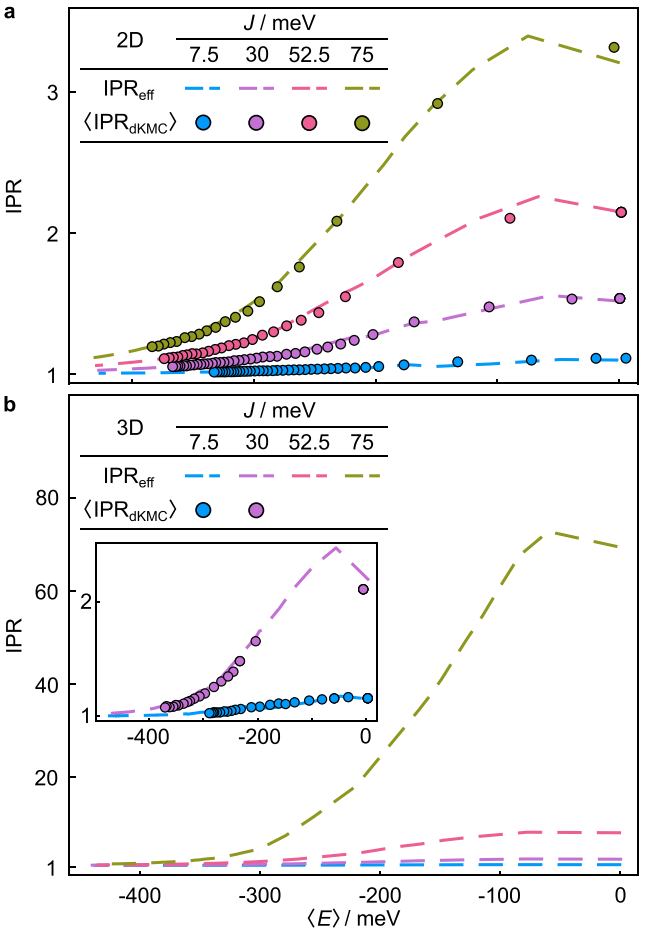

Figure 3. Neighborhood-averaging approach predicts accurate IPRs. In both (a) two and (b) three dimensions, the neighborhood-averaging approach gives the effective IPR (dashed lines) as a function of mean polaron energy $\langle E \rangle$. These results reproduce the mean IPR of occupied states in dKMC (points) obtained using fully dynamical simulations of polarons relaxing in the DOS. The right-most point corresponds to time zero, and subsequent points (toward lower $\langle E \rangle$ and lower IPR) correspond to progressively longer dKMC simulations. The apparent maximum in IPR$_{eff}$ around an $\langle E \rangle$ of −100 meV is a numerical artifact caused by boundary effects when averaging over very small neighborhoods required at energies close to zero; this effect is negligible below approximately $\langle E \rangle$ = −200 meV, which includes the points relevant for this work. Results are calculated for σ = 150 meV, λ = 200 meV, and T = 300 K.

To simulate transport, we initialize a polaron in the center of the lattice and calculate 10 KMC trajectories[1,25] over 10 000 disordered landscapes using the jKMC rate. During these simulations, we track the squared displacement $r^2(t)$ of the polaron and its energy $E(t)$. We average these quantities over the ensemble of trajectories to obtain mean-square displacement $\langle r^2(t) \rangle$ and mean energy $\langle E(t) \rangle$ of the diffusing polaron. We then calculate the mobility at time t_E at which $\langle E(t_E) \rangle = E_\mu$ using

$$\mu(t_E) = \frac{e}{2dk_BT} \frac{\mathrm{d}}{\mathrm{d}t} \langle r^2(t) \rangle \Big|_{t=t_E} \tag{12}$$

where e is the electron charge and d is the dimension.

Before discussing jKMC mobilities, we show that the neighborhood-averaging approach reproduces the mean IPRs obtained from full dKMC calculations (Figure 3). In dKMC, the mean IPR $\langle \mathrm{IPR}_{\mathrm{dKMC}} \rangle$ and mean energy $\langle E_{\mathrm{dKMC}} \rangle$ of the occupied states can be obtained as functions of time by simulating and averaging transport over ensembles of diagonalized polaron landscapes. Therefore, Figure 3 shows that the neighborhood-averaging approach can be used to predict the mean IPR (and, therefore, r_{deloc}) across a wide range of parameters without expensive dKMC calculations.

jKMC reproduces the large delocalization enhancements seen in dKMC over a wide range of electronic couplings (Figure 4a,b). In particular, for the parameters chosen, it reproduces the 2 order of magnitude enhancement over KMC. jKMC can also describe regimes inaccessible to dKMC, especially transport involving large electronic couplings in three dimensions, where it predicts even larger enhancements in mobility.

The delocalization enhancements of jKMC remain large over a range of E_μ in both two and three dimensions (Figure 4c,d). The chosen range of E_μ corresponds to the several order of magnitude differences in transport time t_E (Figure 4e,f), showing that the delocalization enhancement persists over a broad range of time scales. For the parameters tested, jKMC agrees with dKMC to a factor of ∼2. Overall, jKMC provides excellent accuracy considering the simplicity of the method, typical uncertainties in the input parameters, and the fact that the mobilities span orders of magnitude and are underestimated by KMC by as much as 100 times.

The values of r_{deloc} used in jKMC (Figure 4g,h) are within the typical range of its analogue γ^{-1} sometimes used in Marcus or Miller−Abrahams models. For the parameters used in Figure 4, we predict r_{deloc}/a within a range of 0.2−0.6, whereas

https://doi.org/10.1021/acs.jpclett.3c00388
J. Phys. Chem. Lett. 2023, 14, 3757−3764

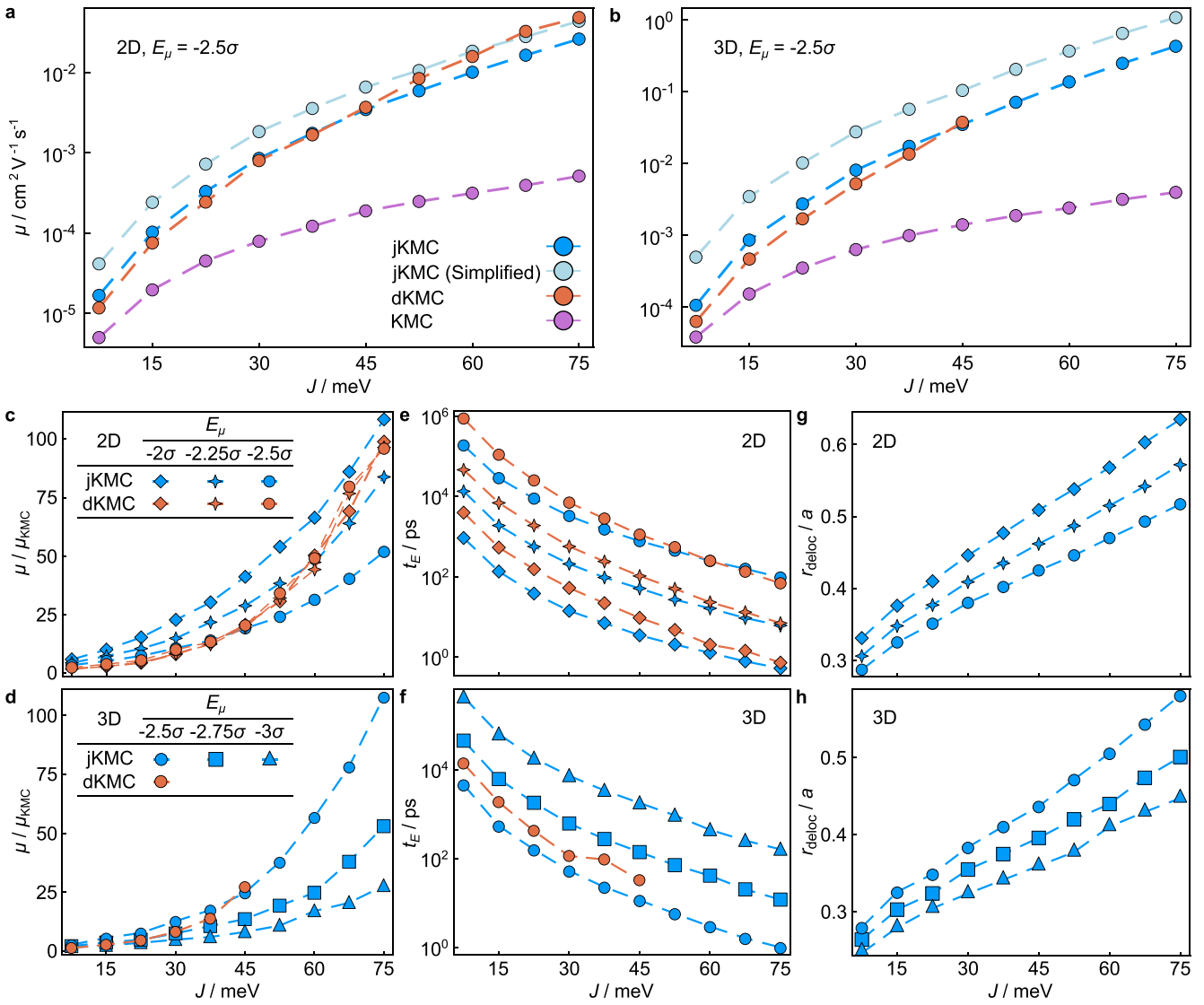

Figure 4. jKMC reproduces the large delocalization enhancements explained by dKMC, including the 2 order of magnitude enhancements in mobility over KMC in (a) two and (b) three dimensions. jKMC reproduces dKMC mobilities where the latter are known and extends beyond them to high levels of delocalization in three dimensions. The simplified jKMC rate also predicts mobilities on the same order of magnitude as dKMC. Mobilities are calculated at $E_\mu = -2.5\sigma$ with σ = 150 meV, λ = 200 meV, and T = 300 K. (c and d) jKMC reproduces the delocalization enhancements of dKMC over KMC across a range of E_μ values to a factor of ∼2. (e and f) Times t_E taken to reach target energy E_μ show that the range of E_μ in panels c and d spans the typical time scales of mesoscopic charge transport. (g and h) Delocalization radii that parametrize jKMC.

the values of γ^{-1}/a are typically in the range of 0.1−1.[28,37] In other words, jKMC is a microscopic justification of phenomenological γ^{-1} parameters that are often inserted into hopping models to enable them to fit experimental results.

Figure 5a shows that the delocalization correction can increase mobilities by several orders of magnitude over KMC hopping (r_{deloc} = 0). In Figure 5a, r_{deloc} is varied independently, isolating its role from those of the other material parameters. The IPRs corresponding to r_{deloc} are shown in Figure 5b, which remain modest for the significant enhancements in mobility.

The results of simplified jKMC are also shown in panels a and b of Figure 4 (and in Figure S3), showing that eq 11 can be an acceptable approximation for typical delocalizations in disordered organic semiconductors. The simplified jKMC rate leads to the same order of magnitude mobilities as dKMC; however, it tends to slightly systematically overestimate jKMC.

Despite its overall accuracy and the ability to predict the correct trends, jKMC has systematic errors in certain regimes. Panels c and d of Figure 4 show jKMC overestimates mobilities on short time scales (shallow E_μ) and underestimates them at long time scales (deep E_μ). These errors are related to the assumption of a uniform polaron size, which neglects the effect of the distribution of polaron sizes on mobility. At short time scales, where the distribution is wide and the effective IPR is large, jKMC overestimates the escape from localized traps. In contrast, on long time scales where the distribution has narrowed and the effective IPR is small, jKMC underestimates the escape from traps into highly delocalized states. The boundary between these regimes depends on coupling J, as shown in panels c and d of Figure 4.

jKMC achieves a computational cost between those of KMC and dKMC. While based on dKMC, jKMC avoids dKMC's computational bottleneck of having to repeatedly diagonalize Hamiltonians during the dynamics. Instead, it requires only an up-front diagonalization to calculate the effective IPR. Furthermore, jKMC can achieve neighborhood averaging by

https://doi.org/10.1021/acs.jpclett.3c00388
J. Phys. Chem. Lett. 2023, 14, 3757−3764

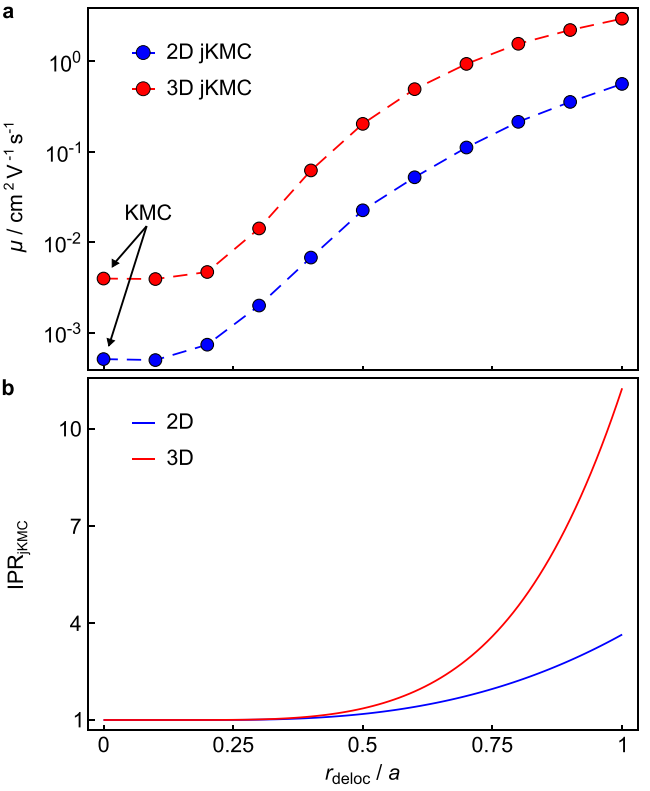

Figure 5. jKMC delocalization correction can produce large increases in mobilities. (a) In both two and three dimensions, varying r_{deloc} independently of J increases the mobility by several orders of magnitude. Therefore, adding delocalization correction $\xi_{\nu\nu'}$ can easily reproduce large mobilities where conventional KMC hopping fails. Results are calculated at $E_\mu = -2.5\sigma$ for $J = 75$ meV, $\sigma = 150$ meV, $\lambda = 200$ meV, and $T = 300$ K. (b) The jKMC IPR depends on only r_{deloc} and can be varied to probe the effect of delocalization. Modest amounts of delocalization produce order of magnitude enhancements in panel a.

diagonalizing fewer and smaller lattices than need to be diagonalized in dKMC. Smaller lattices suffice in jKMC because the effective IPR is heavily weighted toward smaller, lower-energy polarons (see section S4 of the Supporting Information). In contrast, dKMC is designed to calculate the dynamics of any polaron on the lattice, including highly delocalized states that require large lattices to describe. Nevertheless, the up-front diagonalization remains the computational bottleneck of jKMC at high electronic couplings. However, it needs to be done only once before running a routine KMC calculation using jKMC rates.

The approximations in jKMC allow it to demonstrate the important role of delocalization in a wide range of organic semiconductors, and the simplicity of the resulting equations provides clear insight into how the microscopic parameters affect the mesoscopic dynamics. However, most of the approximations could be relaxed to extend jKMC to other regimes.

The distinguishing assumption of jKMC is the uniformly sized spherical polarons, and the assumptions of both uniform size and shape could be relaxed. Polaron sizes could be made non-uniform to capture the distribution of polaron IPRs and their correlation to the polaron energies (i.e., lower-energy states are generally more localized than those in the middle of the DOS). This could be achieved by using a different r_{deloc} for each polaron, as a function of its energy. However, doing so would require both keeping track of the polaron IPR distribution and modifications to hopping rates to account for different initial and final values of polaron r_{deloc}. Similarly, the assumption of spherical polarons could be relaxed without using the raw polaron wave functions obtained by diagonalization. Spherical polarons are appropriate for materials with isotropic couplings; by contrast, anisotropic couplings, such as those in polymers or oligoacene crystals, could be described using ellipsoidal polarons. Doing so would involve incorporating different values of r_{deloc} and J for each spatial direction (e.g., along a polymer chain or between chains), in a manner similar to previous approaches using Marcus and Miller–Abrahams rates.[37]

The high-temperature assumption could also be relaxed, at the cost of losing the simplicity and intuition of jKMC. In particular, it is possible to directly use the sPTRE rates in eq 3 with the spherical polarons of jKMC but without taking the high-temperature limit of $K_{\Delta(ij,i'j')}(\omega)$. These equations are given as intermediate results in section S1 of the Supporting Information.

Other approximations in jKMC are shared by the implementations of the underlying sPTRE and dKMC theories. If they were relaxed, the sPTRE equations of motion might change, which would imply consequent changes in jKMC dynamics. For example, it would be possible to extend jKMC to accommodate long-range electronic couplings, a non-Gaussian DOS,[28,32,41] or spatial site-energy correlations,[28,42] regimes that are rarely explored with sPTRE or dKMC. There are also approximations that are inherited from sPTRE and dKMC. For example, sPTRE assumes fixed electronic couplings, which could be relaxed to include both disordered couplings and off-diagonal fluctuations that can dominate transport in energetically ordered materials.[43,44]

In the future, jKMC will provide the opportunity to determine the effect of delocalization on other optoelectronic processes in disordered materials or on a device level, regimes that would be too complicated to explore using dKMC or any other quantum-mechanical method.[24] For example, we expect that jKMC can be extended to modeling multiple particles, including charge separation and recombination processes. These simulations could be used to parametrize drift-diffusion simulations of delocalized charges, connecting the mesoscopic dynamics to a complete, multiscale device model.

In conclusion, jKMC is a practical model of partially delocalized transport that approaches the accuracy of fully quantum approaches with the cost of classical hopping. jKMC includes a simple correction to the Marcus hopping rate, based on a method for estimating the delocalization radius. It reproduces the large increases in mobility predicted by dKMC but can also simulate larger electronic couplings and delocalization in three dimensions. These factors make jKMC an attractive model that could easily be included in any KMC simulation of a disordered material, including future device-scale models that take into account partially delocalized charge transport.

■ ASSOCIATED CONTENT

Supporting Information

The Supporting Information is available free of charge at https://pubs.acs.org/doi/10.1021/acs.jpclett.3c00388.

https://doi.org/10.1021/acs.jpclett.3c00388
J. Phys. Chem. Lett. 2023, 14, 3757−3764

jKMC rate derivation (section S1), simplified jKMC rate derivation (section S2), simplified jKMC results (mobility enhancements and simulation times) (section S3), and effective IPR convergence (section S4) (PDF)

AUTHOR INFORMATION

Corresponding Author

Ivan Kassal − *School of Chemistry, University of Sydney, Sydney, NSW 2006, Australia;* orcid.org/0000-0002-8376-0819; Email: ivan.kassal@sydney.edu.au

Authors

Jacob T. Willson − *School of Chemistry, University of Sydney, Sydney, NSW 2006, Australia*

William Liu − *School of Chemistry, University of Sydney, Sydney, NSW 2006, Australia;* orcid.org/0000-0003-4306-5851

Daniel Balzer − *School of Chemistry, University of Sydney, Sydney, NSW 2006, Australia;* orcid.org/0000-0002-4640-1059

Complete contact information is available at: https://pubs.acs.org/10.1021/acs.jpclett.3c00388

Notes

The authors declare no competing financial interest.

ACKNOWLEDGMENTS

The authors were supported by the Australian Research Council (DP220103584), by a Westpac Scholars Trust Future Leaders Scholarship, by an Australian Government Research Training Program scholarship, and by computational resources from the Sydney Informatics Hub (Artemis) and the Australian Government's National Computational Infrastructure (Gadi) through the National Computational Merit Allocation Scheme.

REFERENCES

(1) Köhler, A.; Bässler, H. *Electronic processes in organic semiconductors*, 1st ed.; Wiley-VCH, 2015.

(2) Oberhofer, H.; Reuter, K.; Blumberger, J. Charge transport in molecular materials: An assessment of computational methods. *Chem. Rev.* **2017**, *117*, 10319−10357.

(3) Balzer, D.; Smolders, T. J. A. M.; Blyth, D.; Hood, S. N.; Kassal, I. Delocalised kinetic Monte Carlo for simulating delocalisation-enhanced charge and exciton transport in disordered materials. *Chem. Sci.* **2021**, *12*, 2276−2285.

(4) Anderson, P. Absence of diffusion in certain random lattices. *Phys. Rev.* **1958**, *109*, 1492−1505.

(5) Grover, M.; Silbey, R. Exciton migration in molecular crystals. *J. Chem. Phys.* **1971**, *54*, 4843−4851.

(6) Giannini, S.; Carof, A.; Ellis, M.; Yang, H.; Ziogos, O. G.; Ghosh, S.; Blumberger, J. Quantum localization and delocalization of charge carriers in organic semiconducting crystals. *Nat. Commun.* **2019**, *10*, 3843.

(7) Zhang, G.; et al. Delocalization of exciton and electron wavefunction in non-fullerene acceptor molecules enables efficient organic solar cells. *Nat. Commun.* **2020**, *11*, 3943.

(8) Spencer, J.; Gajdos, F.; Blumberger, J. FOB-SH: Fragment orbital-based surface hopping for charge carrier transport in organic and biological molecules and materials. *J. Chem. Phys.* **2016**, *145*, 064102.

(9) Giannini, S.; Carof, A.; Blumberger, J. Crossover from hopping to band-like charge transport in an organic semiconductor model: Atomistic nonadiabatic molecular dynamics simulation. *J. Phys. Chem. Lett.* **2018**, *9*, 3116−3123.

(10) Giannini, S.; Blumberger, J. Charge transport in organic semiconductors: The perspective from nonadiabatic molecular dynamics. *Acc. Chem. Res.* **2022**, *55*, 819−830.

(11) Heck, A.; Kranz, J. J.; Kubař, T.; Elstner, M. Multi-scale approach to non-adiabatic charge transport in high-mobility organic semiconductors. *J. Chem. Theory Comput.* **2015**, *11*, 5068−5082.

(12) Heck, A.; Kranz, J. J.; Elstner, M. Simulation of temperature-dependent charge transport in organic semiconductors with various degrees of disorder. *J. Chem. Theory Comput.* **2016**, *12*, 3087−3096.

(13) Jiang, Y.; Zhong, X.; Shi, W.; Peng, Q.; Geng, H.; Zhao, Y.; Shuai, Z. Nuclear quantum tunnelling and carrier delocalization effects to bridge the gap between hopping and bandlike behaviors in organic semiconductors. *Nanoscale Horiz.* **2016**, *1*, 53−59.

(14) Fratini, S.; Mayou, D.; Ciuchi, S. The transient localization scenario for charge transport in crystalline organic materials. *Adv. Funct. Mater.* **2016**, *26*, 2292−2315.

(15) Nematiaram, T.; Ciuchi, S.; Xie, X.; Fratini, S.; Troisi, A. Practical computation of the charge mobility in molecular semiconductors using transient localization theory. *J. Phys. Chem. C* **2019**, *123*, 6989−6997.

(16) Varvelo, L.; Lynd, J. K.; Bennett, D. I. G. Formally exact simulations of mesoscale exciton dynamics in molecular materials. *Chem. Sci.* **2021**, *12*, 9704−9711.

(17) Li, W.; Ren, J.; Shuai, Z. Finite-temperature TD-DMRG for the carrier mobility of organic semiconductors. *J. Phys. Chem. Lett.* **2020**, *11*, 4930−4936.

(18) Li, W.; Ren, J.; Shuai, Z. A general charge transport picture for organic semiconductors with nonlocal electron-phonon couplings. *Nat. Commun.* **2021**, *12*, 4260.

(19) Savoie, B. M.; Kohlstedt, K. L.; Jackson, N. E.; Chen, L. X.; Olivera de la Cruz, M.; Schatz, G. C.; Marks, T. J.; Ratner, M. A. Mesoscale molecular network formation in amorphous organic materials. *Proc. Natl. Acad. Sci. U. S. A.* **2014**, *111*, 10055−10060.

(20) Jackson, N. E.; Chen, L. X.; Ratner, M. A. Charge transport network dynamics in molecular aggregates. *Proc. Natl. Acad. Sci. U.S.A.* **2016**, *113*, 8595−8600.

(21) Janković, V.; Vukmirović, N. Energy-temporal pathways of free-charge formation at organic bilayers: Competition of delocalization, disorder, and polaronic effects. *J. Phys. Chem. C* **2020**, *124*, 4378−4392.

(22) Jang, S. Theory of multichromophoric coherent resonance energy transfer: A polaronic quantum master equation approach. *J. Chem. Phys.* **2011**, *135*, 034105.

(23) Lee, C. K.; Moix, J.; Cao, J. Coherent quantum transport in disordered systems: A unified polaron treatment of hopping and band-like transport. *J. Chem. Phys.* **2015**, *142*, 164103.

(24) Balzer, D.; Kassal, I. Even a little delocalization produces large kinetic enhancements of charge-separation efficiency in organic photovoltaics. *Sci. Adv.* **2022**, *8*, eabl9692.

(25) Bässler, H. Charge transport in disordered organic photoconductors. A Monte Carlo simulation study. *Phys. Status Solidi B* **1993**, *175*, 15−56.

(26) Marcus, R. A. On the theory of oxidation-reduction reactions involving electron transfer. I. *J. Chem. Phys.* **1956**, *24*, 966−978.

(27) Miller, A.; Abrahams, E. Impurity conduction at low concentrations. *Phys. Rev.* **1960**, *120*, 745−755.

(28) Baranovskii, S. D. Theoretical description of charge transport in disordered organic semiconductors. *Phys. Status Solidi B* **2014**, *251*, 487−525.

(29) Wilken, S.; Upreti, T.; Melianas, A.; Dahlström, S.; Persson, G.; Olsson, E.; Österbacka, R.; Kemerink, M. Experimentally calibrated kinetic Monte Carlo model reproduces organic solar cell current−voltage curve. *Sol. RRL* **2020**, *4*, 2000029.

(30) Zojer, K. Simulation of charge carriers in organic electronic devices: Methods with their fundamentals and applications. *Adv. Opt. Mater.* **2021**, *9*, 2100219.

(31) Upreti, T.; Wilken, S.; Zhang, H.; Kemerink, M. Slow relaxation of photogenerated charge carriers boosts open-circuit voltage of organic solar cells. *J. Phys. Chem. Lett.* **2021**, *12*, 9874−9881.

(32) Vukmirović, N.; Wang, L.-W. Carrier hopping in disordered semiconducting polymers: How accurate is the Miller−Abrahams model? *Appl. Phys. Lett.* **2010**, *97*, 043305.
(33) Jang, S.; Cao, J.; Silbey, R. J. On the temperature dependence of molecular line shapes due to linearly coupled phonon bands. *J. Phys. Chem. B* **2002**, *106*, 8313−8317.
(34) Pollock, F. A.; McCutcheon, D. P. S.; Lovett, B. W.; Gauger, E. M.; Nazir, A. A multi-site variational master equation approach to dissipative energy transfer. *New J. Phys.* **2013**, *15*, 075018.
(35) Wilner, E. Y.; Wang, H.; Thoss, M.; Rabani, E. Sub-Ohmic to super-Ohmic crossover behavior in nonequilibrium quantum systems with electron-phonon interactions. *Phys. Rev. B* **2015**, *92*, 195143.
(36) Brédas, J. L.; Calbert, J. P.; da Silva Filho, D. A.; Cornil, J. Organic semiconductors: A theoretical characterization of the basic parameters governing charge transport. *Proc. Natl. Acad. Sci. U.S.A.* **2002**, *99*, 5804−5809.
(37) Hoffmann, S. T.; Athanasopoulos, S.; Beljonne, D.; Bässler, H.; Köhler, A. How do triplets and charges move in disordered organic semiconductors? A Monte Carlo study comprising the equilibrium and nonequilibrium regime. *J. Phys. Chem. C* **2012**, *116*, 16371−16383.
(38) Shuai, Z.; Li, W.; Ren, J.; Jiang, Y.; Geng, H. Applying Marcus theory to describe the carrier transports in organic semiconductors: Limitations and beyond. *J. Chem. Phys.* **2020**, *153*, 080902.
(39) Melianas, A.; Pranculis, V.; Devižis, A.; Gulbinas, V.; Inganäs, O.; Kemerink, M. Dispersion-dominated photocurrent in polymer:-fullerene solar cells. *Adv. Funct. Mater.* **2014**, *24*, 4507−4514.
(40) Melianas, A.; Kemerink, M. Photogenerated charge transport in organic electronic materials: Experiments confirmed by simulations. *Adv. Mater.* **2019**, *31*, 1806004.
(41) Vissenberg, M. C. J. M.; Matters, M. Theory of the field-effect mobility in amorphous organic transistors. *Phys. Rev. B* **1998**, *57*, 12964−12967.
(42) Gartstein, Y.; Conwell, E. High-field hopping mobility in molecular systems with spatially correlated energetic disorder. *Chem. Phys. Lett.* **1995**, *245*, 351−358.
(43) Troisi, A.; Orlandi, G. Charge-transport regime of crystalline organic semiconductors: Diffusion limited by thermal off-diagonal electronic disorder. *Phys. Rev. Lett.* **2006**, *96*, 086601.
(44) Troisi, A.; Orlandi, G. Dynamics of the intermolecular transfer integral in crystalline organic semiconductors. *J. Phys. Chem. A* **2006**, *110*, 4065−4070.

https://doi.org/10.1021/acs.jpclett.3c00388
J. Phys. Chem. Lett. 2023, 14, 3757−3764

Jumping Kinetic Monte Carlo: Fast and Accurate Simulations of Partially Delocalised Charge Transport in Organic Semiconductors

Supporting Information

Jacob T. Willson, William Liu, Daniel Balzer, and Ivan Kassal
School of Chemistry, University of Sydney, NSW 2006, Australia
** E-mail: ivan.kassal@sydney.edu.au*

S1. JKMC RATE DERIVATION

The foundation of jumping kinetic Monte Carlo (jKMC) is the secular polaron transformed Redfield equation (sPTRE) [1, 2], which provides the hopping rate from any polaron ν to polaron ν' as

$$R_{\nu\nu'} = \sum_{\langle i,j\rangle,\langle i',j'\rangle} 2J^2 \,\mathrm{Re}\left[\,\langle\nu|i\rangle\,\langle j|\nu'\rangle\,\langle\nu'|i'\rangle\,\langle j'|\nu\rangle\,K_{\Delta(ij,i'j')}\left(\omega_{\nu\nu'}\right)\right], \tag{S1}$$

where $\langle i,j\rangle$ and $\langle i',j'\rangle$ are nearest-neighbour pairs of sites, J is the nearest-neighbour electronic coupling, $\omega_{\nu\nu'} = E_\nu - E_{\nu'}$ is the energy difference between polarons, and

$$K_{\Delta(ij,i'j')}(\omega) = \int_0^\infty d\tau\, e^{i\omega\tau}\langle \hat{V}_{ij}(\tau)\hat{V}_{i'j'}(0)\rangle_B \tag{S2}$$

is the half-range Fourier transform of the bath correlation function

$$\langle \hat{V}_{ij}(\tau)\hat{V}_{i'j'}(0)\rangle_B = \kappa^2(e^{-\Delta(ij,i'j')\phi(\tau)} - 1), \tag{S3}$$

where $\Delta(ij,i'j') = \delta_{ii'} - \delta_{ij'} + \delta_{jj'} - \delta_{ji'}$,

$$\kappa = \exp\left(-\int_0^\infty \frac{d\omega}{\pi}\frac{J(\omega)}{\omega^2}\coth\left(\frac{\omega}{2k_\mathrm{B}T}\right)\right), \tag{S4}$$

and

$$\phi(\tau) = \int_0^\infty \frac{d\omega}{\pi}\frac{J(\omega)}{\omega^2}\left(\cos(\omega\tau)\coth\left(\frac{\omega}{2k_\mathrm{B}T}\right) - i\sin(\omega\tau)\right). \tag{S5}$$

We assume that the polaron wavefunctions are identical, spherically symmetric, and exponentially decaying in the site basis,

$$|\nu\rangle = A\sum_i \exp\left(-\frac{d_{i\nu}}{r_\mathrm{deloc}}\right)|i\rangle, \tag{S6}$$

where $d_{i\nu}$ is the distance between the centre of the spherical polaron ν and site i, r_deloc is the delocalisation radius that characterises the size of the wavefunction, and the normalisation prefactor is $A = (\sum_i \exp(-2d_{i\nu}/r_\mathrm{deloc}))^{-1/2}$. Substituting the spherical-polaron approximation into the sPTRE yields

$$R_{\nu\nu'} = \sum_{\langle i,j\rangle,\langle i',j'\rangle} 2J^2A^4\,\mathrm{Re}\left[K_{\Delta(ij,i'j')}\left(\omega_{\nu\nu'}\right)\right]\exp\left(-\frac{d_{i\nu}+d_{j\nu'}+d_{i'\nu'}+d_{j'\nu}}{r_\mathrm{deloc}}\right). \tag{S7}$$

To simplify this expression, we assume the high-temperature limit ($k_\mathrm{B}T \gg \omega_c$) in eq. (S5), using $\coth(\omega/2k_\mathrm{B}T) \approx 2k_\mathrm{B}T/\omega$ to obtain

$$\phi(\tau) = \int_0^\infty \frac{d\omega}{\pi}\,\frac{J(\omega)}{\omega^2}\left(\frac{2k_\mathrm{B}T}{\omega}\cos(\omega\tau) - i\sin(\omega\tau)\right). \tag{S8}$$

$\phi(\tau)$ enters the integral in eq. (S2) through an exponential, meaning that the integral will be dominated by contributions where $\phi(\tau)$ achieves the maximum real values. This maximisation occurs when $\cos(\omega\tau) \approx 1$, i.e., when $\omega\tau \ll 1$. Therefore, we take the Taylor expansions of $\cos(\omega\tau)$ and $\sin(\omega\tau)$ in eq. (S8) to yield

$$\phi(\tau) = 2k_\mathrm{B}Tx_3 - (k_\mathrm{B}T\tau^2 + i\tau)x_1, \tag{S9}$$

where

$$x_n = \int_0^\infty \frac{d\omega}{\pi} \frac{J(\omega)}{\omega^n} \tag{S10}$$

Similarly, the high-temperature limit of eq. (S4) is

$$\kappa^2 = e^{-4k_\mathrm{B}Tx_3}, \tag{S11}$$

which is exponentially small at high T.

Therefore, in the high-temperature limit, the bath correlation function becomes

$$\langle \hat{V}_{ij}(\tau)\hat{V}_{i'j'}(0)\rangle_B = e^{-4k_\mathrm{B}Tx_3}\left(e^{-\Delta(ij,i'j')\left(2k_\mathrm{B}Tx_3-(k_\mathrm{B}T\tau^2+i\tau)x_1\right)}-1\right), \tag{S12}$$

where the coefficient $\Delta(ij,i'j')$ assumes integer values between -2 and 2. Of these, the $\Delta(ij,i'j')=-2$ contributions (i.e., $i=j'$ and $j=i'$) dwarf the others, and are the only ones negative and large enough to ensure that the κ^2

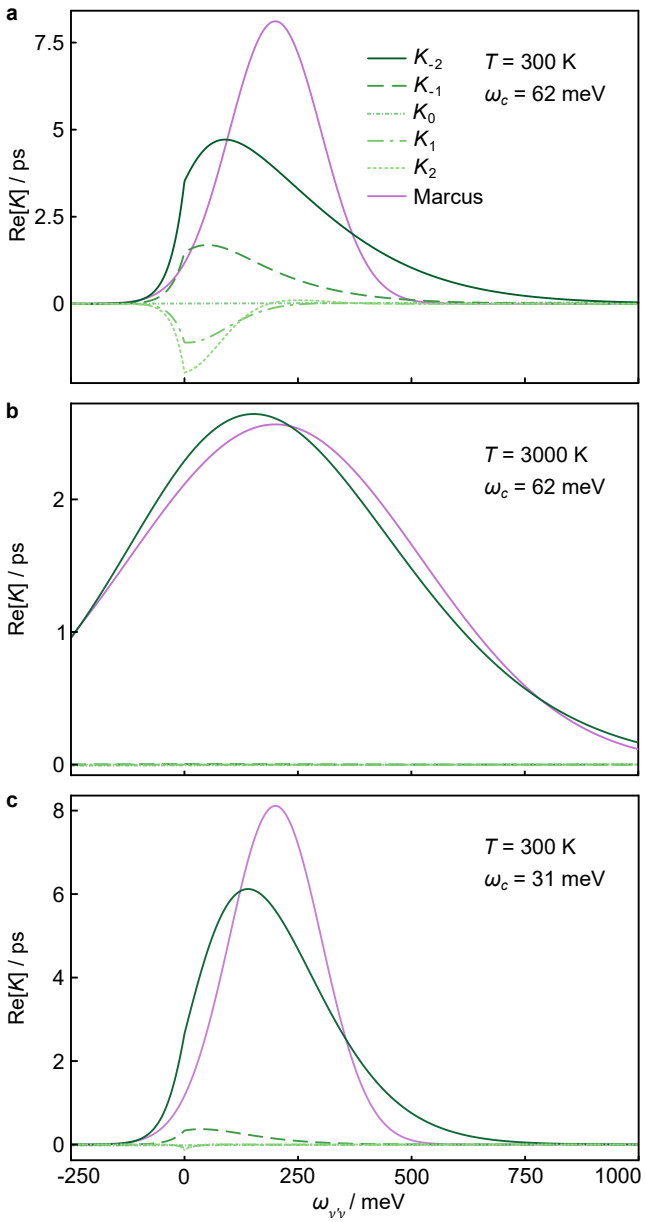

Figure S1. **Comparison of different** $K_{\Delta(ij,i'j')}(\omega)$, shown as functions of the polaron energy difference $\omega_{\nu\nu'}$. Results are calculated using the spectral density $J(\omega)$ given in the main text for $\lambda = 200\,\mathrm{meV}$ and **(a)** the parameters in this work ($T = 300\,\mathrm{K}$, $\omega_c = 62\,\mathrm{meV}$), **(b)** at higher temperature ($T = 3000\,\mathrm{K}$), and **(c)** at lower cutoff frequency ($\omega_c = 31\,\mathrm{meV}$). At high temperatures or low cutoff frequencies, four of the five $K_{\Delta(ij,i'j')}(\omega)$ become negligible, and the surviving $K_{-2}(\omega)$ approaches $k_\mathrm{Marcus}(\omega)/2J^2$ (shown in purple).

prefactor does not make the entire expression exponentially small in T. In the high-temperature limit, the other four possibilities of $\Delta(ij, i'j')$ give negligible results, as shown in fig. S1. Keeping only the $\Delta(ij, i'j') = -2$ terms in eq. (S7) yields

$$R_{\nu\nu'} = 2J^2A^4 \operatorname{Re}\left[K_{-2}\left(\omega_{\nu\nu'}\right)\right] \sum_{\langle i,j\rangle} \exp\left(-\frac{2(d_{i\nu} + d_{j\nu'})}{r_{\text{deloc}}}\right), \tag{S13}$$

where

$$K_{-2}(\omega) = \int_0^\infty d\tau\, e^{i\omega\tau}\left(e^{-2k_{\text{B}}T\tau^2 x_1 - 2i\tau x_1} - e^{-4k_{\text{B}}Tx_3}\right). \tag{S14}$$

This expression can be further simplified by neglecting the last term (which is small at high T), by noting that $2x_1 = \lambda$ (the definition of reorganisation energy), and by extending the lower limit of the integral to $-\infty$ (because the real part of the integrand is even) to give

$$\begin{aligned}
\operatorname{Re}\left[K_{-2}(\omega)\right] &= \frac{1}{2}\int_{-\infty}^{\infty} d\tau\; e^{i(\omega-\lambda)\tau} e^{-\lambda k_{\text{B}}T\tau^2} \\
&= \sqrt{\frac{\pi}{4\lambda k_{\text{B}}T}} \exp\left(-\frac{(\omega-\lambda)^2}{4\lambda k_{\text{B}}T}\right) \\
&= \frac{k_{\text{Marcus}}(\omega)}{2J^2},
\end{aligned} \tag{S15}$$

where k_{Marcus} is the Marcus hopping rate. Substituting this expression for $K_{-2}(\omega_{\nu\nu'})$ into eq. (S13) gives eq. (9) in the main text.

S2. SIMPLIFIED JKMC RATE DERIVATION

The delocalisation correction $\xi_{\nu\nu'}$ for hopping between polarons ν and ν' can be simplified in the limit of low delocalisation to yield the simplified jKMC rate. As described in the main text,

$$\xi_{\nu\nu'} = A^4 \sum_{\langle i,j\rangle} \exp\left(-\frac{2(d_{i\nu} + d_{j\nu'})}{r_{\text{deloc}}}\right). \tag{S16}$$

For small r_{deloc}, the sum of exponentials in eq. (S16) is dominated by the terms that minimise the distance $d_{i\nu} + d_{j\nu'}$, where i and j are nearest neighbours. As shown in fig. S2, there are $d_{\nu\nu'}/a$ dominant terms with the minimal $d_{i\nu} + d_{j\nu'} = d_{\nu\nu'} - a$. Because $A = 1$ in the limit of localised charges, we obtain the simplified jKMC delocalisation correction

$$\xi^{\text{Simplified}}_{\nu\nu'} = \frac{d_{\nu\nu'}}{a} \exp\left(-\frac{2\left(d_{\nu\nu'} - a\right)}{r_{\text{deloc}}}\right). \tag{S17}$$

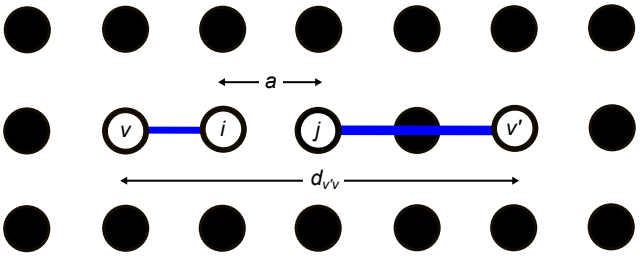

Figure S2. **The arrangement of sites whose contribution dominates the jKMC rate.** The dominant terms in the sPTRE minimise the distance $d_{i\nu} + d_{j\nu'}$ (shown in blue). On the cubic lattice, the simplest case is if the initial and final states ν and ν' lie in the same row (or column) of the lattice, as shown above. In that case, there are $d_{\nu\nu'}/a$ positions for the nearest-neighbours i and j which minimise this distance to $d_{\nu\nu'} - a$, and which occur when all four points are collinear. We use the same result ($d_{\nu\nu'}/a$ positions with total distance $d_{\nu\nu'} - a$) even if ν and ν' do not lie in the same row or column. This approximation is justified because the particular shape of the lattice is not an essential part of the jKMC model.

S3. SIMPLIFIED JKMC RESULTS

The mobility enhancements and times taken to reach the target energy E_μ for simplified jKMC are shown in fig. S3.

S4. EFFECTIVE IPR CONVERGENCE

Figure S4 shows that the lattices diagonalised in jKMC can be much smaller than those in dKMC. Smaller lattices are much easier to diagonalise, giving jKMC a significant computational advantage over dKMC.

REFERENCES

[1] Jang, S. Theory of multichromophoric coherent resonance energy transfer: A polaronic quantum master equation approach. *J. Chem. Phys.* **2011**, *135*, 034105.

[2] Lee, C. K.; Moix, J.; Cao, J. Coherent quantum transport in disordered systems: A unified polaron treatment of hopping and band-like transport. *J. Chem. Phys.* **2015**, *142*, 164103.

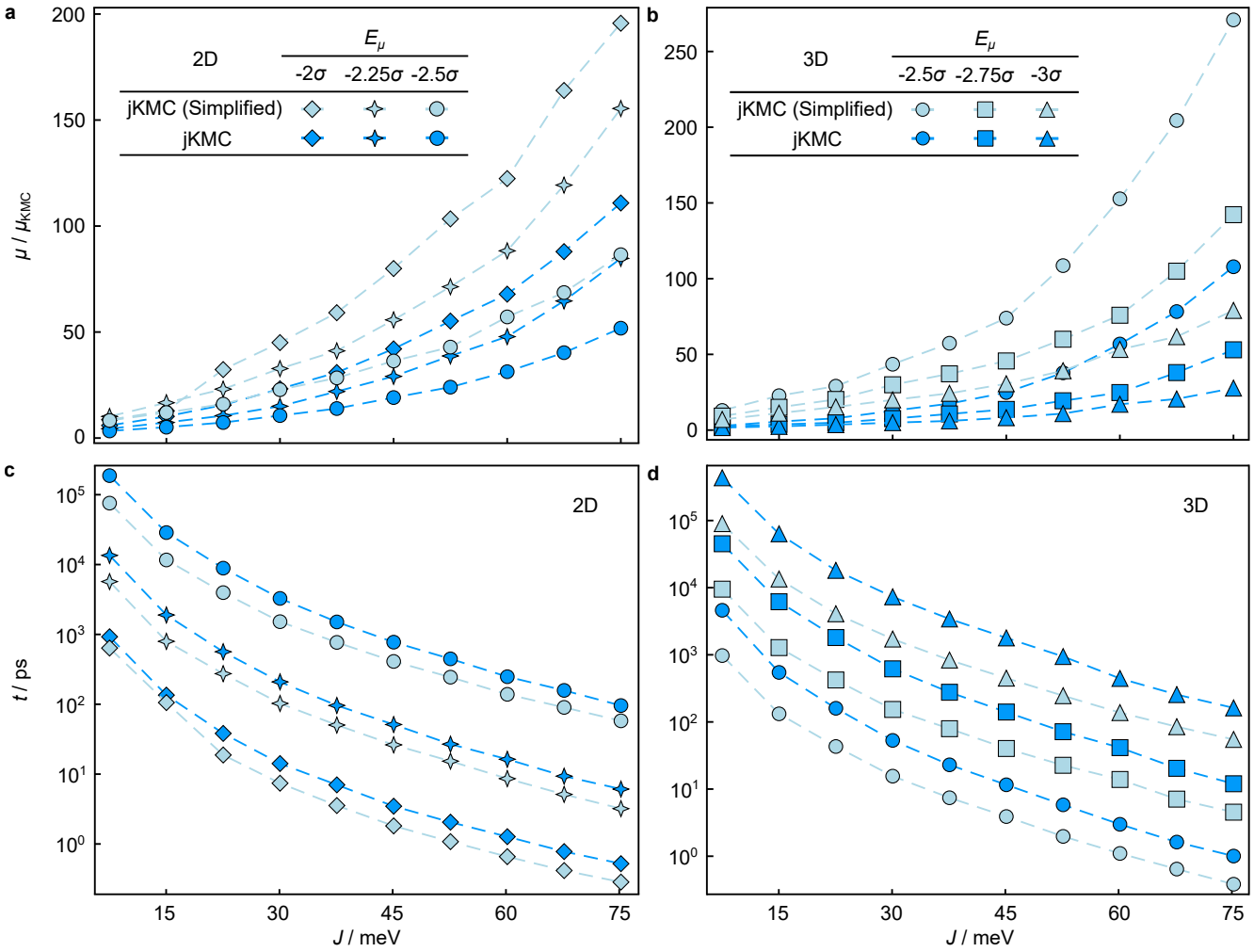

Figure S3. **Simplified jKMC produces mobilities on the same order of magnitude as jKMC.** In both **(a)** two and **(b)** three dimensions, simplified jKMC reproduces jKMC mobilities to about a factor of 2 (for the parameters tested), but tends to systematically overestimate them. Results are calculated for $\sigma = 150\,\text{meV}$, $\lambda = 200\,\text{meV}$, and $T = 300\,\text{K}$. **(c,d)** The corresponding times taken to reach the target energy E_μ using simplified jKMC.

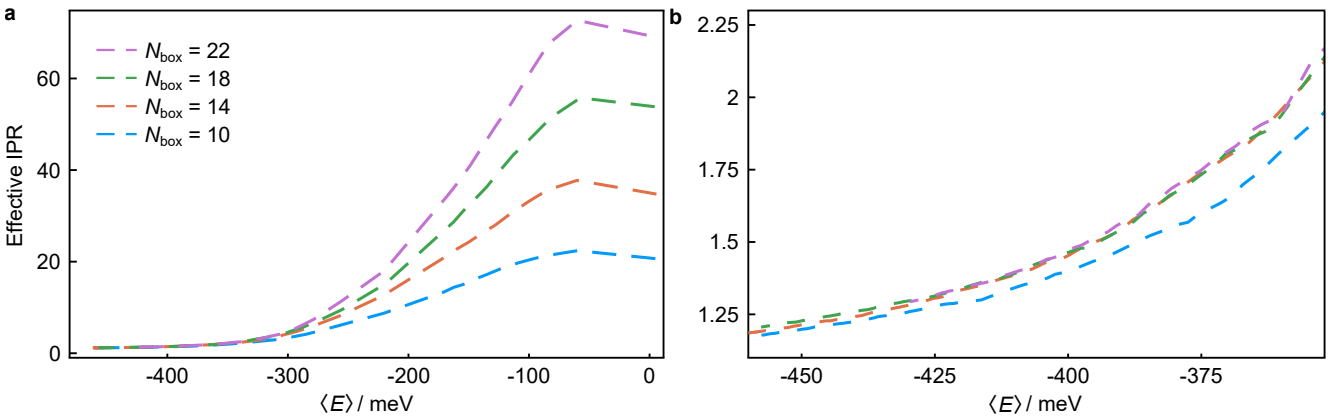

Figure S4. **Calculations of effective IPRs at deep $\langle E \rangle$ converge rapidly as a function of lattice size.** The effective IPR in d dimensions is calculated using the neighbourhood-averaging method on a lattice of size N_{box}^{d}. **(a)** Calculations of the effective IPR converge when N_{box} is large enough to accommodate the sizes of the delocalised polaron states that contribute to transport at $\langle E \rangle$. Here, $N_{\mathrm{box}} \approx 20$ is sufficient for convergence for $\langle E \rangle$ below about $-300\,\mathrm{meV}$. By contrast, dKMC requires boxes large enough to converge the mean IPR of all states, corresponding to $\langle E \rangle = 0$, which would require substantially larger N_{box}. **(b)** Enlarged view of panel **a** for the values of $\langle E \rangle$ considered in this paper. Here, smaller N_{box} suffice to achieve convergence because the effective IPR is a thermal average, mostly sensitive to low-energy, localised states that are adequately described using small lattices. Results are shown for three dimensions, $J = 75\,\mathrm{meV}$, $\sigma = 150\,\mathrm{meV}$, $\lambda = 200\,\mathrm{meV}$, and $T = 300\,\mathrm{K}$.